2
3
4
5
6
7
8

A global summary of seafloor topography influenced by internal-wave induced turbulent water mixing

16
17
18

by Hans van Haren and Henk de Haas

23
24
25
26
27
28
29
30
31
32

34 NIOZ Royal Netherlands Institute for Sea Research, P.O. Box 59, 1790 AB Den Burg,
35 the Netherlands.
36 e-mail corresponding author: hans.van.haren@nioz.nl

39   Short summary. Turbulent water motions are important for the exchange of momentum, heat,

40   nutrients, and suspended matter in the deep-sea. The shape of marine topography influences

41   most water turbulence via breaking internal waves at 'critically' sloping seafloors. In this

42   paper, the concept of critical slopes is revisited from a global internal wave-turbulence

43   viewpoint using seafloor topography- and moored temperature sensor data. Potential

44   robustness of the seafloor-internal wave interaction is discussed.

45

46   **Abstract.** Turbulent water motions are important for the exchange of momentum, heat,

47   nutrients, and suspended matter including sediments in the deep-sea that is generally stably

48   stratified in density. To maintain ocean-density stratification, an irreversible diapycnal

49   turbulent transport is needed. The geological shape and texture of marine topography is

50   important for water mixing as most of deep-sea turbulence is generated via breaking internal

51   waves at sloping seafloors. For example, slopes of semidiurnal internal tidal characteristics

52   can 'critically' match the mean seafloor slope. In this paper, the concept of critical slopes is

53   revisited from a global internal wave-turbulence viewpoint using seafloor topography- and

54   moored high-resolution temperature sensor data. Observations suggest that turbulence

55   generation via internal wave breaking at 5±1.5% of all seafloors is sufficient to maintain

56   ocean-density stratification. However most, >90%, turbulence contribution is found at

57   supercritical, rather than the more limited critical, slopes measured at 1′-scales that cover

58   about 50% of seafloors at water depths < 2000 m. Internal tides (~60%) dominate over near-

59   inertial waves (~40%), which is confirmed from comparison of NE-Atlantic data with East-

60   Mediterranean data (weakno tides). Seafloor-elevation spectra show a wavenumber (k) fall-

61   off rate of k^{-3}, which is steeper than previously found. The fall-off rate is even steeper,

62   resulting in less elevation-variance, in a one-order-of-magnitude bandwidth around k_T=0.5

63   cycle-per-km. The corresponding length is equivalent to the internal wavetidal excursion

64   length. The reduction in seafloor-elevation variance seems associated with seafloor-erosion

65   by internal wave breaking. Potential robustness of the seafloor and -internal wave interaction

66   is discussed.

67

1 Introduction

The present ocean exists for millions of years, and so seemingly do its seafloor shape and its water flows including properties like the stable vertical stratification in density from the heating by the sun. Because sedimentation and erosion of suspended matter in the ocean are subject to water flows that partially depend on interaction with the seafloor, one may question the stability or variability of seafloor-shape and water flow properties. Compared with geological time scales of variation (sedimentary: years; rocks: centuries/millennia), water flows in the deep ocean are fast fluctuating (meso-scale eddies: weeks/months; tides: hours/days). However, that does not preclude potential interactions between water flows and topographic bed-forms, with local results such as sand ripples and sediment waves (e.g., Trincardi and Normark, 1988; Puig et al., 2007).

As seafloor-erosion by resuspension is mainly driven by intense water turbulence, and seafloor-deposition by weak turbulence, seafloor-shaping such as contourite morphology (e.g., Rebesco et al. 2014; Chen et al., 2022) depends on dominant ocean-turbulence generation processes. Following, e.g., Wunsch (1970), Eriksen (1982), Thorpe (1987), Klymak and Moum (2003), Hosegood et al. (2004) and Sarkar and Scotti (2017), ocean turbulence above sloping seafloors is predominantly generated via the breaking of internal water waves. The turbulence produced by the breaking of internal waves is considered vital for the global ocean meridional overturning circulation (e.g., St. Laurent et al., 2012). Such waves are mainly supported by the stable vertical density stratification. Their effects on shaping ocean's seafloor morphology cannot be overestimated (Rebesco et al., 2014).

More in general, balancing feed-back interaction leading to a quasi-stable equilibrium is expected between the slopes of seafloor topography and long-lasting ubiquitous water-flows, e.g., generated by internal waves that are notably driven by oscillating tides and the waves' density-stratification support. In their pioneering works, Bell (1975a,b) from an internal wave generation perspective, Cacchione and Wunsch (1974) and Eriksen (1982; 1985) from an internal wave breaking perspective, and Cacchione and Southard (1974) from a geological

95 formation perspective, suggested that a 'critical' match exists between the mean angles of

96 deep-sea topography slopes and those of internal wave 'characteristics'.

97   Because internal water waves are essentially three-dimensional (3D) phenomena, which

98 distinguishes them from 2D surface waves, their energy propagates along characteristics, i.e.

99 paths that slope to the horizontal as a function of wave frequency and stratification. Internal

100 waves can reflect off a seafloor slope, but due to angle-preservation with respect to gravity

101 instead of bottom-normal internal wave energy is thought to build-up when the two slopes are

102 identical, yielding potential propagation parallel to a critical seafloor slope (Cacchione and

103 Wunsch, 1974). When the seafloor slope is larger than the internal wave slope it is

104 supercritical, when it is smaller than the internal wave slope it is subcritical (for that particular

105 wave frequency under given stratification conditions).

106   While Bell (1975a,b) considered seafloor elevation statistics on internal wave generation,

107 the works by Cacchione and co-authors considered seafloor shaping by internal wave

108 motions. It was found that the average seafloor slope amounts $3\pm1°$, which matches the

109 characteristics slope of energy propagation direction of internal waves at semidiurnal tidal

110 frequency for stratification from around 1700 m below the sea surface, which is about half the

111 average water depth.

112   While the above finding is remarkable and has led to numerous investigations on critical

113 reflection of internal waves, it is challenged from various perspectives. This is because: First,

114 exactly matching 'critical' slopes for dominant internal tides are few and far between and

115 cannot persist in space and time because the ocean stratification varies in space and time.

116 Second, internal waves mostly break above sloping topography, very little in the ocean

117 interior (Polzin et al., 1997). Third, most ocean seafloors, i.e. 75% by area and 90% by

118 volume (Costello et al., 2010; Costello et al., 2015), occur between 3000 and 6000 m water

119 depth where density stratification is weak. Fourth, about 40% of total internal wave energy is

120 estimated at near-inertial frequencies (e.g., Wunsch and Ferrari, 2004).

121   Near-inertial waves are generated as transients following geostrophic adjustment on the

122 rotating Earth, e.g., after passing atmospheric disturbances or frontal collapses (LeBlond and

Mysak, 1978). Their occurrence shows a strong variability with location, e.g., demonstrating large near-surface generation in western boundary flows and much weaker generation in eastern ocean-basins (Watanabe and Hibiya, 2002; Alford, 2003). As near-inertial waves have a quasi-horizontal component, virtually all seafloor slopes are steeper: They are super-critical (for near-inertial waves). These observations demand further investigation in the seafloor/internal wave-turbulence interaction, also considering the potential impact on climate variability and the contribution of oceans in distributing heat therein.

Detailed ocean observations indicate that most intense turbulence and sediment resuspension over sloping seafloors is not generated by frictional (shear-)flows (as suggested by, e.g., Cacchione et al., 2002), but by nonlinearly deformed internal waves breaking (e.g., Klymak and Moum, 2003; Hosegood et al., 2004). Such nonlinear internal wave breaking predominantly generates buoyancy-driven convection-turbulence. Growing evidence suggests that most breaking occurs at slopes that are just supercritical (van Haren et al., 2015; Winters, 2015; Sarkar and Scotti, 2017).

Any interaction between seafloor shape and texture and water-flow turbulence is expected to vary on geological time scales, because besides deep-sea topography also ocean-interior vertical density stratification exists as long as the oceans do: The ocean is not and has not been a pool of stagnant cold water underneath a thin layer of circulating warm water heated by the sun (Munk and Wunsch, 1998). The question is how stable a balance of such an interaction can be, e.g., between internal waves that are supported by varying stratification and seafloor topography. Is the balance an optimum, or rather a marginal equilibrium, like the marginally stable stratification supporting maximum destabilizing internal shear in shelf seas (van Haren et al., 1999)? Especially given relatively rapid changes, such as Earth-surface heating attributed to mankind, does a balance buffer any modifications: to topography (long time scale), vertical density stratification (medium time scale), and/or to water-flow (short time scale)? Prior to being able to (mathematically) predict any potential tipping point of a balance, the physical processes need to be understood that contribute to a balance. Amongst

150   other deep-sea processes, this involves the physics of internal wave-formation and -breaking

151   into turbulence generation upon interaction with topography and restratification of density.

152   In this paper, we discuss the (im)possibility of relating seafloor statistics with open-ocean

153   density stratification and internal wave breaking as observed in recent measurements. We

154   revisit concepts of deformation, erosion, and sedimentation, of deep seafloor topography in

155   interaction with internal waves, with vertical density stratification, with turbulence, with

156   ocean's heating/cooling, and consider the (in)stability of these interactions. Instead of Bell's

157   (1975a,b) perspective of internal wave generation, above NE-Pacific abyssal hills, we adopt

158   the perspective of internal wave breaking and turbulence generation through moored high-

159   resolution temperature observations above a wide variety of deep-ocean topography. We also

160   adopt a geological seafloor topography perspective using some detailed multibeam

161   echosounder and global seafloor elevation repository data. An attempt is made to consider the

162   statistical spread of different variables.

163

164   *1.1 Some considerations on ocean variability and internal wave-topography interactions*

165   A large variability over two orders of magnitude exists in stable ocean-density

166   stratification ($\sim N^2$), albeit a gradual, not constant, decrease with increasing depth is observed

167   in buoyancy frequency N, a measure of stability of a fluid to vertical displacements (e.g.,

168   Wüst, 1935; Wunsch, 2015). This gradual decrease with depth results in a corresponding

169   increase in the slope β to the horizontal of characteristics along which internal wave energy

170   propagates. For general ocean stratification this slope is approximately inversely proportional

171   to N (e.g., LeBlond and Mysak, 1978),

172        $\beta = \sin^{-1}((\omega^2 - f^2)^{1/2} / (N^2 - f^2)^{1/2})$,   (1)

173   for freely propagating linear internal waves at frequency ω. Here, f denotes the inertial

174   frequency or Coriolis parameter, the vertical component of planetary vorticity. Internal waves

175   and sub-inertial water-flows deform the stratification locally, thereby making N a function of

176 time and space $N = N(x,y,z,t)$. The consequences of variability for β will be explored from

177 observations in Section 3.

178   Several global internal wave statistics can be given. The rms-mean deep-sea topography

179 slopes of $3\pm1°$ (Bell, 1975b; Cacchione et al., 2002) roughly match the mean slope of (linear)

180 semidiurnal internal tide characteristics, provided the latter are computed using in (1) a value

181 of $N \approx 2\times10^{-3}$ s^{-1} for mid-latitude locations. Such N is found approximately around $z = -1700$

182 m in the open ocean, which has a mean depth of $H = 3900$ m outside shelf seas (Wunsch,

183 2015). In these open-ocean mid-depth waters internal wave breaking and thus turbulence

184 generation are sparse (e.g., Gregg, 1989; Polzin et al., 1997; Kunze, 2017).

185 Observational evidence suggests that vigorous turbulent mixing by internal wave

186 breaking is only found in a limited height of $h = 100\text{-}200$ m (e.g., Polzin et al., 1997) above

187 the seafloor, coarsely estimated to occur over only 5-15% of all seafloor slopes to maintain

188 the ocean stratification (e.g., van Haren et al., 2015). As for relevant length scales: Although

189 satellite altimetry observations demonstrate low-mode internal tides having wavelengths

190 $O(100)$ km (e.g., Dushaw, 2002; Ray and Zaron, 2016), the excursion length of internal tides

191 is typically $O(1)$ km and which may prove important for turbulence generation and thus

192 sediment erosion of seafloor-texture and -topography.

193 Especially the smaller length scale $O(1)$ km may fit the spectral analysis of NE-Pacific

194 seafloor elevation, which is found to fall-off with horizontal wavenumber (k) like $k^{-2.5}$ (Bell,

195 1975a), later corrected to k^{-2} (Bell, 1975b). The latter is interpreted as a random distribution

196 of hills in which the energy of formation is distributed uniformly over all sizes. Internal wave

197 generation is found by Bell (1975a,b) mainly between $0.33 < k < 3$ cpkm (short for cycles per

198 kilometer). Here, we add that this roughly matches a ~~spectral~~ band with increased spread of

199 topographic-height variance ~~broadening~~ between $0.15 < k < 1$ cpkm, which is visible in the

200 presented data albeit not mentioned by Bell (1975a,b).

201 Geomorphology influences water-flow and turbulence and these in turn influence

202 sediment erosion and deposition and thus (fine-tuning) the geomorphology. So, if enough

203   time is available (after all, geologists think in terms of millions of years), one will eventually

204   reach an equilibrium. The major geomorphological processes occur on a much larger

205   timescale than the adaptation of water-flows, and any ocean will "always" be in an

206   equilibrium situation because the flows adapt relatively quickly to a slow geological change.

207   Thus, following variations in ocean internal wave turbulence, seafloor topography will

208   adapt. However, the ocean also interacts with a faster adaptive/varying system: the

209   atmosphere. Temperature changes in water are slower than in air because of the larger heat

210   capacity of the former. Nevertheless, a direct correspondence with changes in vertical density

211   (temperature) stratification is not evident as larger stratification can support more internal

212   waves and thus potentially more turbulent wave breaking that may restore a balance. (It is

213   noted that atmosphere dynamics is not driven by the ocean, except indirectly by modification

214   of moisture content).

215   The dominant source of ocean internal waves are tides (e.g., Wunsch and Ferrari, 2004).

216   The local seafloor slope γ, computed over a ~~certain~~~~particular~~ horizontal distance, is

217   supercritical for linear freely propagating semidiurnal lunar M_2 internal tidal waves, when $\gamma >$

218   β_{M2}, using $\omega_{M2} = 1.405 \times 10^{-4}$ s^{-1} in (1).

219   A secondary source are near-inertial waves $\omega \approx f$, which generally have a near-horizontal

220   slope of characteristics. Only in very weak stratification $N = O(f)$, some near-inertial slopes

221   may become large enough to distinguish various subcritical slopes for such waves. However,

222   under weakly stratified conditions, terms involving the horizontal Coriolis parameter are no

223   longer negligible, and two distinctly differently sloping characteristics $\mu_\pm$ of internal wave

224   energy propagation result (e.g., LeBlond and Mysak, 1978; Gerkema et al., 2008):

225        $\mu_\pm = (B \pm (B^2 - AC)^{1/2})/A,$ (2)

226   in which $A = N^2 - \omega^2 + f_s^2$, $B = ff_s$, $C = f^2 - \omega^2$ and $f_s = f_h \sin\alpha$, α the angle to latitude (φ). The

227   slopes of $\mu_\pm$ indicate directions to the horizontal in a more general way than the single slope

228   (1) obtained under the traditional approximation.

229   For large N >> f, the slope of the two characteristics in (2) approach each other and their

230   slope approaches β in (1). Under conditions N < 10f and latitudinal propagation (α = π/2),

231   one of the characteristics in (2) becomes quasi-horizontal for which virtually all seafloor

232   slopes are supercritical, and the other becomes more steeply sloping.

233   The impact of (2) may also not be ignorable for semidiurnal tides in weakly stratified

234   waters around mid-latitudes. With the full non-approximated equations (2) and a stratification

235   of about N = 8f, which is typical in waters near the 3900-m mean depth of the ocean seafloor,

236   the slope (1) of β_{M2} = 9.1° rather becomes 10.3° and 7.9° for up- and down-going

237   characteristics $\mu_{\pm}$, respectively (for |φ| = 37°).

238   This spread of about ±13% is a substantial addition to variation in seafloor slope-

239   criticality and becomes larger at weaker stratification (N < 8f) and smaller at stronger

240   stratification (N > 8f). Although the vertical density stratification is generally a monotonic

241   decreasing function with increasing depth, deviations occur, such as in some, e.g. equatorial,

242   areas around 4000 m where larger N is found than above and below, and which is attributed

243   to the transition between deep Arctic waters overlying most dense Antarctic waters (King et

244   al., 2012).

245   The ubiquitous linear internal waves at various frequencies f ≤ ω ≤ N (for N > f) provide

246   ample options for wave-wave and wave-topography interactions. While some interactions

247   seem too slow, the wave-topography interactions above sufficiently steep topography show

248   strongly nonlinear wave deformation resulting in convection-turbulence when the ratio of

249   particle velocity (u) over phase speed (c) amounts u/c > 1: A fast process. Propagation of such

250   highly nonlinear internal waves is beyond the scope here, but the turbulence dissipation rate

251   of internal wave energy affecting seafloor sediment is not.

252   Although the ocean and deep-seas are overall turbulent in terms of large bulk Reynolds

253   numbers Re well exceeding Re > 10^4 and more generally Re = $O(10^6)$, it is a challenge to

254   study the dominant turbulence processes. As the ocean is mainly stably stratified in density,

255   which hampers the vertical size-evolution of fully developed three-dimensional isotropic

256 turbulence, it is expected that in the deep-sea and in strained thick layers stratification is much

257 weaker resulting in near-neutral conditions of (almost) homogeneous waters in which N ≈ f.

258 Under such conditions turbulent overturns may be slow and large and may govern more the

259 convection-turbulence process, rather than the shear-turbulence process that dominates under

260 well-stratified conditions N >> f across thin layers in the interior and in frictional flows over

261 the seafloor.

262

263

264 *1.2 Internal wave energy dissipation perspective*

265 According to Wunsch and Ferrari (2004), in follow-up from Munk and Wunsch (1998),

266 the currently best estimate for global internal wave power to be dissipated is 0.8 TW (1 TW

267 $=10^{12}$ W) for internal tides and about 0.5 TW for wind-enforced mainly near-inertial waves.

268 These numbers are determined to within an error of a factor of 2, although this error range is

269 probably smaller for internal tides (since the rather precise determination of energy loss of the

270 Moon-Earth system).

271 If we distribute this amount of power over the entire global ocean with a surface of

272 3.6×10^{14} m^2 (e.g., Wunsch, 2015), the vertically integrated dissipation rate amounts for

273 internal tides,

274 2.2×10^{-3} W m^{-2} = $\int \rho \varepsilon$ dz, (3)

275 and 6~~7~~0% of that value for inertial waves. In (3), ρ = 1026 kg m^{-3} denotes an average density

276 of ocean-water and ε the kinetic energy turbulence dissipation rate.

277 If we suppose that (3) is distributed over the entire vertical water column, over a mean

278 water height of H = 3900 m (Costello et al., 2010; Wunsch, 2015), a global mean rate to

279 dissipate the internal tidal energy is required of,

280 $\varepsilon_H = 6 \times 10^{-10}$ m^2 s^{-3}, (4)

281 and 6~~7~~0% of this value for near-inertial waves. As a result, the entire global-mean turbulence

282 dissipation rate of all internal waves (generated by internal tides and near-inertial waves) is

283 about 10^{-9} m^2 s^{-3}. This is equivalent to the mean value found after evaluation of 30,000 ocean

284 profiles on internal wave turbulence (Kunze, 2017).

285 Given a mean mixing efficiency of $\Gamma = 0.2$ over values distributed over one order of

286 magnitude (Osborn, 1980; Oakey 1982; Dillon, 1982), and $N = 1.5\times10^{-3}$ s^{-1} found around

287 open-ocean $z = -1900$ m, one arrives at a vertical (actually, diapycnal) turbulent diffusivity of

288 $K_z = \Gamma\varepsilon N^{-2} = 10^{-4}$ m^2 s^{-1}, for above global internal-wave-induced dissipation rate. This is the

289 canonical K_z-value proposed by Munk (1966) and Munk and Wunsch (1998) to maintain the

290 ocean stratification and to drive the meridional overturning circulation.

291 However, according to measurements using extensive shipborne water column profiling

292 (e.g., Gregg, 1989; Kunze, 2017) and some moored high-resolution temperature sensors (van

293 Haren, 2019) the average open-ocean dissipation rate amounts $4\pm2\times10^{-10}$ m^2 s^{-3}, which is less

294 than half the required value to maintain the ocean stratification. Locations are thus sought

295 where turbulent mixing is sufficiently strong to cover at least 6×10^{-10} m^2 s^{-3} for the

296 insufficient turbulent mixing by sparse internal wave breaking in the open-ocean interior.

297 It has been suggested that >99% of overall internal wave induced ε is to be found for -

298 $2000 < z < -380$ m (Kunze, 2017), reasoning that in this depth zone stratification, $N^2 \propto \varepsilon/K_z$,

299 is largest. However, ε and K_z are not necessarily (un)related, and more complex

300 correspondence has been observed between the three parameters ε, K_z and N, e.g., in Mount

301 Josephine data (van Haren et al., 2015). Above particularly sloping seafloors, turbulence

302 dissipation rate is found to increase with depth (e.g., Polzin et al., 1997; van Haren et al.,

303 2015; Kunze, 2017), with consequences for the outcome of general ocean circulation models

304 with predicted subtle effects on upwelling near the seafloor (Ferrari et al., 2016). The internal

305 wave breaking potency above the abundant seafloor topography led Armi (1979) and Garrett

306 (1990) to propose that one-and-a-half orders of magnitude larger turbulence than found in the

307 ocean-interior would be needed in a layer O(100) m above all seafloors. This suggestion did

308 not include the particulars of dependency of internal wave turbulence intensity on

309 stratification, slopes, and wave-nonlinearity.

310   Internal waves, in particular internal tides, have amplitudes of several tens of meters,

311   which in the vicinity of sloping topography may grow over 50 m, whereby they deform

312   nonlinearly. So, if we suppose a breaking zone of h = 100 m, one needs above all seafloors

313   local turbulence intensity of the value of ε_H augmented by a factor of H/h = 3900/100,

314    $\quad \varepsilon_h = 2.3 \pm 0.7 \times 10^{-8} \ \text{m}^2 \ \text{s}^{-3}.$ \hfill (5)

315   This value has been observed above a (semidiurnal tidal) critical slope around H = 2500 m

316   of Mount Josephine, NE-Atlantic Ocean (van Haren et al., 2015). But, not all seafloor-slopes

317   show the same level of internal wave breaking, and variations in turbulence dissipation rate

318   by a factor of 100 have been observed between sub- and supercritical slopes over horizontal

319   distances of only O(10) km.

320   Potential high-turbulence locations are supercritical slopes (Winters, 2015; van Haren et

321   al., 2015; Sarkar and Scotti, 2017) and canyons (van Haren et al., 2022), where moored

322   observations demonstrate one order of magnitude larger tidally averaged values than ε_h of,

323    $\quad \varepsilon_{ho} = 3.5 \pm 1 \times 10^{-7} \ \text{m}^2 \ \text{s}^{-3},$ \hfill (6)

324   due to internal tidal and near-inertial wave breaking across a larger observational height of h_o

325   = 200±50 m above seafloors around H = 1000±200 m. About 60% of turbulence dissipation

326   rate occurs in half an hour during the passage of an upslope propagating bore with 50-m

327   averaged peak intensities of $10^{-5} \ \text{m}^2 \ \text{s}^{-3}$ (van Haren and Gostiaux, 2012).

328   If such turbulence intensity as in ε_{ho} occurs in 250/3900 of mean water depth it needs to

329   occur over only 5±1.5% of all slopes to sustain 1.67 times ε_H. The percentage-value is the

330   mean of statistical distribution accounting for errors. This ~5% is still a considerable portion

331   of the ocean's seafloors. If just by internal tides, because virtually all seafloors are

332   supercritical for near-inertial waves, supercritical slopes are required to comprise 3±1% of the

333   slopes, according to ε_H. In half-shallower waters of H = 1900 m, these percentages of slopes

334   are reached for similar turbulence intensity over h = 125 m, but these shallower water depths

335   present only about 10% of the ocean seafloor area (Costello et al., 2010; Costello et al., 2015).

336   We elaborate in Section 3. It is noted that we require (just) supercritical slopes for intense

337 turbulent internal wave breaking, not critical slopes that are limited over (much) smaller areas

338 and are prone to vary more with space and time than supercritical slopes.

339

340 *1.2.1 Variability in linear internal waves*

341 Considering the limited occurrence of critical slopes, we address the variability in internal

342 (tidal) wave slopes (1), $\beta = \beta(\omega, f, N, t)$. At a fixed mooring location, planetary f '(f^p') has

343 zero variability, but relative rotational vorticity of up to $f^r = \pm 0.05 f^p$ may be introduced by

344 (sub-)mesoscale eddy activity, so that f should be replaced by 5% variable local effective

345 Coriolis parameter $f^{eff} = f^p + f^r$ (e.g., Kunze, 1985). Likewise, different semidiurnal tidal

346 internal wave frequencies lead to a~~n, e.g. spring-neap,~~ variation of slopes. Because solar

347 frequency S_2 differs by 3.5% from lunar M_2, $\Delta\beta(\omega)$ varies by about 6% around mean β. (It is

348 noted that internal M_2 cannot propagate freely very far poleward of $|\varphi| \Rightarrow 74.5°$ under

349 stratified conditions using non-approximated equations: to $|\varphi| < 76.5°$ for N = 2f, < 75° for N

350 = 4f, and < 74.5° for N = 100f). Natural variability in density stratification can be~~,~~ caused by a

351 complex of varying flows at internal wave, (sub-)mesoscale, seasonal, and decadal scales.

352 This leads to variations in ~~mean~~ 100-m-scale- N of 5-10% and to local variations of up to 20%

353 in small-scale stratification layers: A lot depends on the particular vertical length scale used in

354 the computation of N. It is noted that stratification~~,~~ ~~which~~ should last at least a buoyancy- and

355 better an inertial period, to be distinguished from turbulent overturns.

356 Summing up, overall variations of 10% in β are common for linear semidiurnal internal

357 tides. The associated variation of characteristics slope angle of 0.5°, for mean N = 10f, yields

358 a vertical variation O(100) m over a horizontal distance of 10 km. These amounts double

359 when non-traditional effects (2) are considered.~~, and thereby become of the same order of~~

360 ~~magnitude as the typical internal tidal excursion length.~~ A precise localization of persistent

361 "critical" slopes is therefore not possible.

362 From a geological perspective one may question how, and in what stable equilibrium the

363 shape of topography exists, as internal wav~~tid~~es depend on frequency and latitude, but

364 foremost on underwater vertical density stratification. In addition, (linear) internal tides can

365 deform after interaction with other internal waves such as those generated at over-tidal(-

366 harmonic), near-inertial and near-buoyancy frequencies.

367

368

369

370 *1.3 Sedimentary topography-slope perspective*

371 ~~A challenge from geological perspective.~~ According to Cacchione et al. (2002), in follow-

372 up from Cacchione and Southard (1974), internal tides are the prime candidate for shaping the

373 ocean's underwater topography, notably its average slope that has approximately the same

374 value as the slope of internal tide characteristics. This is reasoned from the observation that,

375 beyond continental shelves, the average seafloor-slope closely (critically) matches internal

376 tidal characteristics slopes for mean $N \approx 2 \times 10^{-3}$ s^{-1} around mid-latitudes. Cacchione et al.

377 (2002), considering the upper 1000 m of the ocean mainly, assume N is constant at greater

378 depths, which ignores the continued gradual decrease with increasing depth. However, as will

379 be demonstrated in Section 3, ocean's volume-weighted mean N is three times smaller than

380 the mean value above.

381 Cacchione et al. (2002) postulate that sediment erosion, and thus prevention of sediment

382 deposition, occur at slopes where the semidiurnal internal tidal slope critically matches that of

383 topography. The internal-wave model by Cacchione and Wunsch (1974) suggests that for

384 such matching slopes the near-bottom flow is strongest. However, their 1D model is based on

385 low vertical mode linear internal waves, adopting only bed shear-stress as means for

386 (inhibition of) resuspension of sediment. Thereby, the effect of plunging breaking waves is

387 not considered (For the effects on sedimentation resuspension due to better known surface

388 wave breaking, see: Voulgaris and Collins, 2000), besides neglects of spring-neap variability,

389 stratification variability and 3D-effects of topography.

390 As for seafloor topography, the advancement of observational techniques including

391 multibeam acoustic echosounder and satellite altimetry have considerably improved mapping

392 (e.g., Smith and Sandwell, 1997). Using such maps, a global ocean seafloor indexation has

393 been compiled to an overall resolution of 1′ (1852 m in latitude) by Costello et al. (2010). An

394 interesting finding of theirs concerns the separation of ocean area and volume per depth zone.

395 (A correction to area and volume calculations is published in Costello et al. (2015), including

396 a proper definition of depth zone). Whilst 11% of the ocean area and <1% of its volume is

397 occupied by water depths <1000 m, the remarkable results are for the deep sea. It is found that

398 75% of the area and 90% of its volume are in the depth zone with water depths between 3000

399 < H < 6000 m. A large part of this depth zone can be found in the abyssal hill's areas of the

400 Pacific and Atlantic oceans. Only 4.4% of the ocean area and 1.9% of its volume are occupied

401 by the depth zone with water depths between 1000 < H < 2000 m. So, too little topography is

402 in the depth zone of mean N to maintain ocean stratification following the reasoning around

403 ε_{ho}. Expanding to a depth zone of 100 < H < 2000 m, the values are 10% and 2.3%,

404 respectively. We recall that it is the sloping seafloor where most internal waves break and

405 generate turbulence, not the ocean-interior.

406
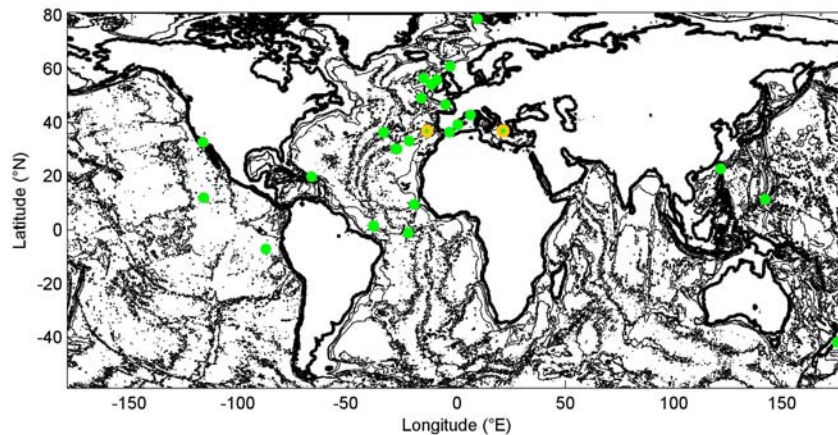
407 **Fig. 1**. Global map of seafloor topography (1′-version of Smith and Sandwell, 1997) with

408 contours every 1500 m together with sites (green dots) of NIOZ T-sensor moorings for

409 deep-sea turbulence and internal wave research of which contributions to mean values are

410 used. The two orange encircled sites are discussed in some detail.

411

412 **2 Materials and methods**

413   The foundation of topography-internal wave interaction leading to our ocean turbulence

414   investigation has been an almost three decades-long observational program of a traveling

415   mooring including instrument development and manufacturing. At some 25 sites (Fig. 1)

416   distributed over the global ocean of varying topographic slopes one or more vertical mooring

417   lines were deployed holding custom-made high-resolution low-noise temperature (T-)sensors

418   (van Haren, 2018). The sites showed a large variety in seafloor topography, from abyssal

419   plains to steep canyons, deep trenches, fracture zones, narrow ridges, large continental slopes,

420   and seamounts. Here, sites shallower than continental shelves are not considered, and specific

421   topics like internal wave interaction with sediment waves are not treated (for an example of

422   such see, e.g., van Haren and Puig, 2017).

423

424   *2.1 Moored T-sensors*

425   Some NE-Atlantic sites like Mount Josephine, Rockall Trough and Faeroer-Shetland

426   Channel were occupied with one or more moorings multiple times. The mooring lengths

427   varied between 30 and 1130-m long strings holding a range of 30-760 stand-alone T-sensors

428   at 0.5-2 m intervals, starting between 0.5 and 8 m from the seafloor. The duration of

429   underwater deployment was at least five days, typically several months, and up to three years.

430   The typical mooring was 100-150 m high with 100 T-sensors and was underwater for several

431   months, sampling at a rate of once per second, resulting in the resolution of most energy-

432   containing internal wave and turbulence scales. This allowed for calculation of turbulence

433   values that were averages over most of the relevant scales, in the vertical and over at least

434   inertial and tidal periods include spring-neap cycle. All moorings were held tautly upright

435   after optimizing sufficient buoyancy and low-drag lineables, for near-Eulerian measurements.

436   All T-sensors were synchronized every 4 hours to a standard clock, so that vertical profiles

437   were measured almost instantaneously within 0.02 s.

438   The main purpose of the moored T-sensors was to infer turbulence values using the

439   sorting method of Thorpe (1977) over deep-sea topography under varying conditions of

440   elevation, stratification, and local water-flow. The moored instrumentation and data

441 processing are extensively described elsewhere (e.g., van Haren and Gostiaux, 2012; van

442 Haren, 2018). Average turbulence dissipation rate values have been used in Section 1.

443   Near every mooring, one or more shipborne water column profiles were made using a

444 Conductivity-Temperature-Depth (CTD) package, mainly SeaBird-911. The CTD-data are

445 used to establish the local temperature-density relationship around the depth-range of moored

446 T-sensors, and for reference of absolute temperature and large-scale stratification.

447

448 *2.2 Seafloor elevation data*

449   Topographic data are retrieved from external data depositories following pioneering

450 works by Smith and Sandwell (1997). Such depositories are GEBCO (https://www.gebco.net)

451 and EMODnet (https://emodnet.ec.europa.eu/en/bathymetry). These data are distributed to

452 grids, e.g., GEBCO-2023 to 15″ (463 m in latitude, North-South direction), and are

453 composites of data from satellite altimetry, shipborne single- and multi-beam acoustic

454 echosounders, and from numerical estimates. Progress is made from the manual soundings of

455 a century ago, via acoustic single-beam echosounder profiling tracks used by Bell (1975a,b),

456 to present-day multibeam mapping and composite global mapping of 1′ (Costello et al., 2010)

457 and smaller. Although the depositories rapidly fill with new high-resolution topographic data

458 following modern multibeam surveys, less than 25~~10~~% of the seafloor has been mapped at a

459 resolution   O(10-100)   m   so   far.   The   UN-decade   initiative   SEABED2030

460 (www.seabed2030.org) aims to complete seabed mapping of the entire ocean before 2030, a

461 challenging goal. It will take at least several decades before the entire seafloor has been

462 mapped at this resolution, if ever. It is noted that the 1′-resolution in some remotely sampled

463 areas results from extrapolated data, while other areas are sampled at 10-100 times higher

464 resolution.

465   Here, we investigate in some detail topography at two specific sites (Fig. 2) of NE-

466 Atlantic Mount Josephine and E-Mediterranean West-Peloponnese using a variety of 15″-

467 resolution GEBCO data, in conjunction with 3.75″ (116 m in latitude) resolution EMODnet

468 data, and about 1.6″ (50 m in latitude) and 0.375″ (11 m in latitude) resolution multibeam

469 data. The latter are obtained locally around the T-sensor mooring sites only. Our multibeam

470 data are de-spiked and somewhat smoothed reducing the original sampling rate by a factor of

471 two approximately. The scale variations allow for a limited investigation in slope dependence

472 on horizontal scales.

473   Although the multibeam echosounder surveys were only a support-part of respective

474 research cruises and therefore do not cover large areas, their extent is sufficient to resolve all

475 internal wave scales. As a bonus, multibeam data processing also delivers information on the

476 reflective properties of the substrate in the property of acoustic backscatter strength. This

477 information was used by van Haren et al. (2015) to demonstrate that over Mount Josephine

478 hard substrates consisting of coarse grain sizes and/or compacted sediment were almost

479 exclusively found in areas with seafloor slopes that were supercritical for semidiurnal internal

480 tides. Less reflective soft substrates consisting of fine grain sizes and/or water-rich sediment

481 were found at sub-critical slopes.
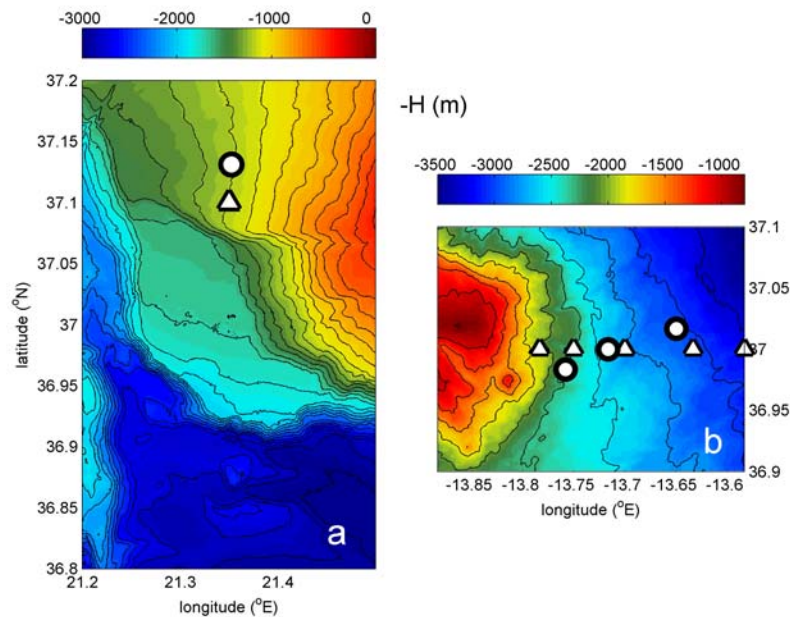
482
483   **Fig. 2**. Two detailed maps made by shipborne multibeam echosounder. (a) Part of West-

484 Peloponnese continental slope, Greece, East-Mediterranean Sea, from R/V Meteor.
485 CircleBlack dot indicatess moored T-sensor location, trianglestar indicates yoyo-CTD
486 station. Black contours are drawn every 100 m. (b) Part of eastern slope of Mount
487 Josephine, Northeast-Atlantic Ocean, from R/V Pelagia. Circles indicate moored T-sensor
488 locations, triangles indicate CTD stations during various years. Black contours are drawn
489 every 250 m.
490
491   The x-y 2D-gridded, being essentially 3D with z included, seafloor elevation data from
492 above sources will be investigated spectrally, to compare with the 1D -single- track,
493 essentially 2D with z included, data from NE-Pacific hills explored by Bell (1975a,b). Some
494 slope statistics is also pursued after computation of the proper slope at each 2D-gridded data-
495 point to characterize the ratio (percentage) of slopes exceeding a particular value. From the
496 total number n_{tot} of 2D-gridded data points per area, we calculate for a particular seafloor
497 slope angle value γ_n, the percentage n/n_{tot} of number n of slopes for which $\gamma > \gamma_n$. Its
498 distribution will be compared with that of internal wave, i.c. semidiurnal internal tide, wave
499 characteristics (1), (2) as a function of N, plotted against the ratio of N over the maximum
500 value N_{max} of N.
501
502
503 *2.3 Analysis methods*
504   Excursion length,
505   $L_e = UT/\pi,$ (7)
506 is induced by oscillatory particle velocities Usin($2\pi t/T$) over time t, where U, T represent
507 flow speed and -period, respectively. As near-inertial wave period T_f varies with latitude, the
508 two specific sites demonstrate,
509   $T_f(|37°|) = 1.8T_{M2},$ (8)
510 As a result, for given identical flow speed the inertial excursion length will be 1.8 times larger
511 than that of semidiurnal internal tide. Nonlinear waves may have different lengths. Excursion
512 lengths will be compared with topography elevation spectra below.

513   As internal wave propagation depends strongly on N, for given latitude and wave

514 frequency, seafloor slopes occurrence statistics should be compared with the ocean's volume-

515 weighted stratification, instead of using vertically averaged N. For ocean volume V(z) per

516 depth zone [z+0.5Δz, z-0.5Δz] roughly every Δz = 1000 m as defined in Costello et al. (2010;

517 2015), a volume weighted buoyancy frequency N_v is calculated as,

518    $N_v(z) = N(z)V(z)/<V>$,   (9)

519 where <…> denotes averaging over the entire vertical water column.

520

521 **3 Results**

522   The two small deep-sea areas for in-depth investigation are around the same mid-latitudes

523 but otherwise distinctly different (Fig. 2). The NE-Atlantic is known for dominant

524 semidiurnal internal tides besides an-order-of-magnitude smaller amplitude near-inertial

525 waves (van Haren et al., 2016). The East-Mediterranean lacks substantial tides so that internal

526 waves are dominated at near-inertial frequencies only. In the NE-Atlantic, sampling sites are

527 above the eastern side of large underwater Mount Josephine, about 400 km West of Southern

528 Portugal. In the East-Mediterranean, the site is about 20 km West of Peloponnese, Greece.

529

530 *3.1 Vertical profiles*

531   The shipborne water column CTD observations demonstrate moderately stratified and

532 seldom homogeneous waters in the lower 300 m above the seafloor when $N = N_{10}$ is

533 computed over small-scale 10-m vertical scales (Fig. 3a). To get some idea of variability of

534 layering in the ocean, $N = N_{100}$ 100-m scale profiles are given for the NE-Atlantic area in Fig.

535 3b, for comparison. Such variability in length-scale dependent layering is similar in the lower

536 400 m above seafloor in the two areas.

537   In the lower 250 m above seafloor of the East-Mediterranean site, the variability in N-

538 profiles becomes larger than in the interior above, with average values slowly decreasing with

539 depth (Fig. 3a). In the lower 100 m above the seafloor the variability in stratification is

540 largest, both in the vertical and in time. The lower 400 m above the seafloor demonstrate

541 >100 m averaged values of $\langle N_{10} \rangle$ = 7±6×10^{-4} s^{-1}, with a gradual decrease of values from 8 to

542 6×10^{-4} s^{-1} towards the seafloor.

543 Similar mean N-values are observed above Mount Josephine at three times greater depth.,

544 but near mean At H = 3900 m, where $\langle N_{100} \rangle$ = 7±2×10^{-4} s^{-1} is observed in the lower 400 m

545 above the seafloor (Fig. 3b). The observed errors and natural variations in N are about twice

546 larger than sketched in Section 1.2. At a given pressure level howeverThus, the NE-Atlantic

547 site is about half-one order of magnitude more stratified, 2-3 times larger in buoyancy

548 frequency, at a given pressure level compared to the East-Mediterranean, and may thus

549 support more internal wave-energy and -shear.

550
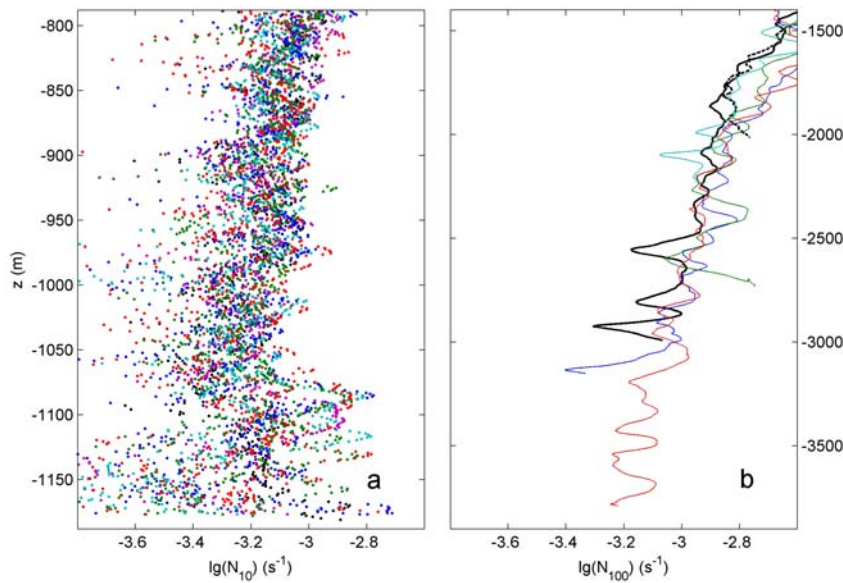
551 **Fig. 3**. Logarithm of buoyancy frequency from shipborne water column CTD. (a) One inertial

552 period of 400-m high yoyo-CTD hourly profiles, 19 in total. Computations are made over

553 10-m vertical scales from fixed location at H = 1180 m water depth in the East-

554 Mediterranean. For clarity, the short-scale profiles are given by coloured dots. (b) Vertical

555 range of 2500 m of profiles from area in (van Haren et al., (2015). Computations are made

556 over 100-m vertical scales down to 10 m from various seafloor depths of the eastern slope

557 of Mount Josephine, NE-Atlantic. X-axis scale is identical, but Y-axis scale is different

558 compared to a.

559

At the deepest NE-Atlantic site considered here, albeit having the mean ocean water depth, the bottom slope is generally subcritical for internal tides (van Haren et al., 2015). This results from the gradual decrease of stratification with depth that leads to a steepening of internal wave characteristics following (1), (2) while the seafloor slope generally becomes smaller for concave topography. To become (super)critical for semidiurnal internal tides, the local slope would need to be (larger than) about 10°.

The (semidiurnal tidal) supercritical portion found above Mount Josephine between 1000 < H < 2300 m (van Haren et al., 2015) may be part of the 5% of surface-area required to maintain the ocean stratification following ε_H. However, it is not sufficient alone, as this required 5% is larger than, albeit within one standard deviation from, the global total of 4%-surface area of depth zone 1000 < H < 2000 m (Costello et al., 2010; 2015). Because also not all slopes between 1000 and 2000 m are expected to be supercritical (for semidiurnal internal tides even under $N > 2 \times 10^{-3}$ s^{-1}; Recall that basically all slopes are supercritical for particularly directed near-inertial waves), other supercritical slopes are sought. Supercritical slopes are more easily found at 100-2300 m relatively shallow depths, given the statistically larger N and thus smaller (1), (2), and sufficient turbulence by internal wave breaking.

How and whereat shapedo internal waves shape the seafloor? Either the seafloor--shape is concave formed by erosion mid-slope, which, given the general mean stratification profile, leads to less likelihood of turbulent mixing due to internal wave breaking in the deep, or it is convex by erosion above and below, which may favour deeper, supercritical slopes and associated enhanced stretches of mixing. Following nonlinear internal wave 2D-modelling, no distinct difference in turbulence intensity is found between internal wave breaking at convex, concave, or planar slopes (Legg and Adcroft, 2003). However, their model results show relatively large values of energy dissipation at sub-critical slopes, which are not found in ocean observations (e.g., van Haren et al., 2015). It is noted that the above modeling is based on 2D spatial-shapes and ocean topography is essentially 3D, like internal wave propagation

586 and turbulence development. It is thus more generalizing to use full 3D seafloor elevation, i.e.

587 full 2D-slope statistics, and evaluate internal wave breaking with that. While near continental

588 margins, where the continental shelf dives into the continental slope around $H = 200$ m, the

589 seafloor generally has a convex shape, it generally becomes concave at greater depths. Such

590 topography would favour relatively shallow supercritical slopes (for semidiurnal internal

591 waves).

592

593 *3.2 Seafloor spectra*

594   The multibeam echosounder data (Fig. 2) allow for local seafloor investigations, in

595 particular on scale-size and -slopes, that go beyond those of Bell (1975a,b) who used single-

596 beam echosounder data resolving height elevations at horizontal scales $O(100)$ m, with a

597 cutoff at Nyquist wavenumber of about $k_{Nyq} = 2.5$ cpkm. Bell (1975a,b) established a general

598 seafloor-elevation spectral fall-off rate of k^n, $-2 < n < -5/2$, for $k_0 < k < k_{Nyq}$, with a smaller

599 slope $-1 < n < 0$ for $k = k_0 < 0.1$ cpkm and flattening $n = 0$ for $k < 0.01$ cpkm.

600   Our multibeam, EMODnet and GEBCO data-sets show a significantly steeper general

601 fall-off rate in elevation spectra (Figs. 4a, 5a) than in Bell (1975a,b), with dominant low-

602 wavenumber fall-off at a rate of about $-k^{-3}$, and a saturation to noise values for $k > 10$ cpkm.

603 The steeper spectral fall-off rates may be interpreted as a deviation from random distribution

604 of seafloor elevation, in which energy is no longer uniformly distributed but favoured at the

605 low-wavenumber side and reduced at the high wavenumber side. It has an intermittent

606 appearance (Schuster, 1984).

607   In detail, the range between $\sim 0.3 < k < \sim 2$ cpkm shows the steepest fall-off rates k^n, $n < -$

608 3, in the East-Mediterranean (Fig. 4), and with extended steep slopes between $\sim 0.55 < k < \sim 6$

609 cpkm in the NE-Atlantic (Fig. 5). The shift of steep-slope range to higher wavenumbers in the

610 NE-Atlantic area approximately corresponds with the shorter excursion lengths for

611 semidiurnal tides compared to inertial waves following (7), (8), for the same flow speeds. The

612 roll-off to weaker slopes for low wavenumbers is barely resolved, although the spectra do

613   show the same tendency as in Bell (1975a,b). Extended GEBCO_2023-data across the Mid-

614   Atlantic Ridge do resolve and show the roll-off at low wavenumbers (not shown).

615

616

617
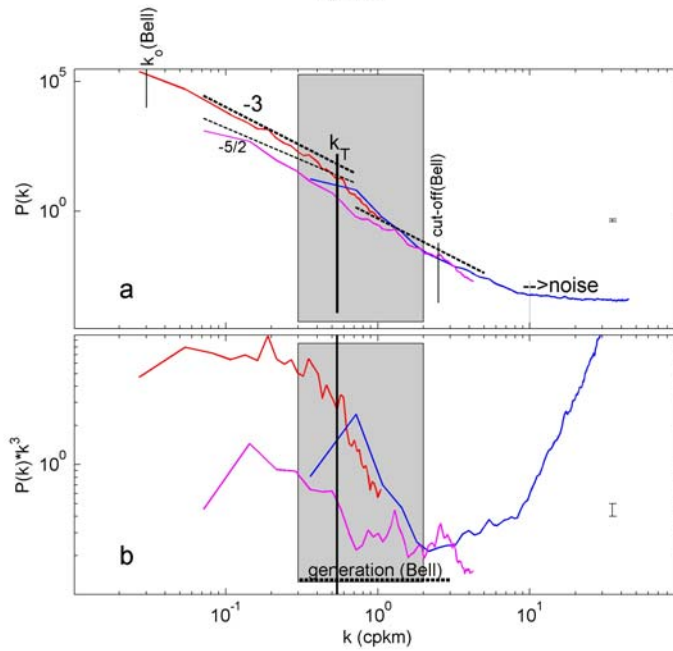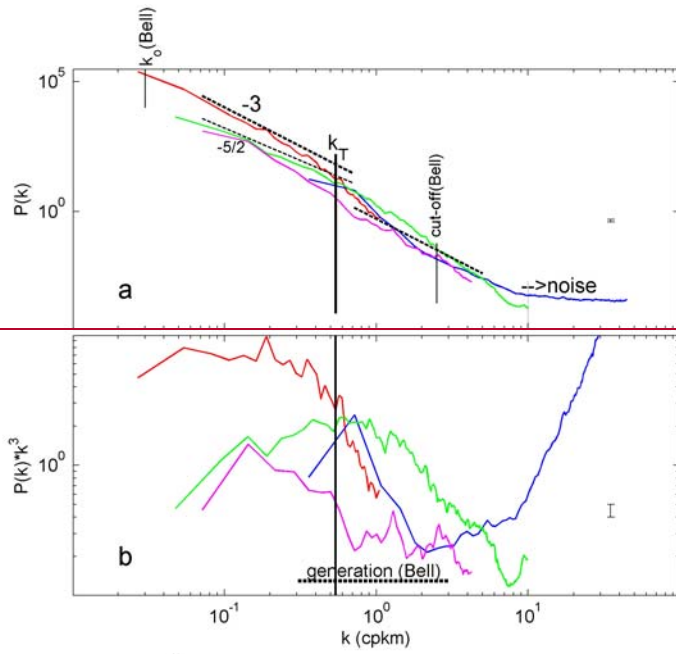
Fig. 4. Spectral analysis of seafloor elevation as a function of horizontal wavenumber k (the inverse of horizontal length-scale L). (a) On the log-log plot matching k⁻³ (-3 on log-log plot) spectral slopes are represented by straight lines, with k⁻⁵/² (-5/2-slope) the slope

621 reported by Bell (1975a). Bell's low-wavenumber cut-off k_0 is indicated, albeit barely

622 resolved, as well as high wavenumber roll-off to noise k_0. The central vertical line at

623 transient wavenumber k_T indicates a wavelength of 1852 m (1′ in latitude). The ~~green plot~~

624 ~~is for 1.6″ sampled Mount Josephine (NE-Atlantic) multibeam data, the~~ three ~~other~~ spectra

625 are for the East-Mediterranean, averages over Fig. 2a: 0.375″ = 11 m sampled multibeam

626 data (blue), 3.75″ = 115 m sampled EMODnet data (magenta), and 15″ = 463 m sampled

627 GEBCO data (red). The grey shading indicates the steep-slope range in which n < -3, for

628 k^n. (b) The same as a., but spectra scaled with k^{-3}, the dominant low wavenumber slope.

629 Bell (1975a,b)'s one-decade range of internal wave generation of Pacific abyssal hills is

630 indicated.

631
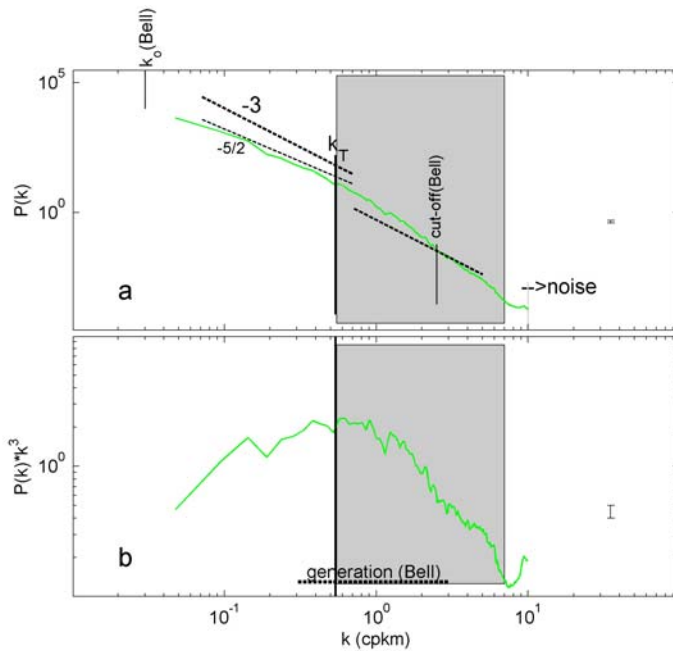
632 **Fig. 5**. As Fig.4, but for 1.6″ = 49 m sampled Mount Josephine (NE-Atlantic) multibeam data,

633 average over Fig. 2b. All straight lines are the same as in Fig. 4, but the shaded area is not.

634

635 The steepest fall-off rate is best visible after scaling the spectra, with k^{-3} in Figs. 4b, 5b, to

636 better indicate this slump-down in seafloor elevation. Noting that this slump-down does not

637 indicate a spectral gap, the range of strong (steeper) deviation before resuming n = -2.5 or -3

638 centers around ~~(tidal)~~ transition wavenumber $k_T \approx 0.5$ cpkm, i.e. a wavelength of $L_T \approx 2$ km. It

639 lies in the range of elevation-variance spreadband broadening that is visible in the data of Bell

640 (1975a,b), and which overlaps with the range of internal wave generation in the abyssal NE-

641 Pacific.

642   Here, it indicates a loss of seafloor topography variance at wavenumber $k > k_T$, by about

643 one order of magnitude (measuring the wavenumber range between the two $n = -3$ spectral

644 slopes). As the k_T associates with that of the largest internal wave (excursion) scales, one may

645 speculate that the loss of slope elevation relative to general fall-off rate is related with low-

646 frequency internal waves, semidiurnal internal tides, mainly, or near-inertial waves having

647 larger period (8) than M_2-tides at $|\varphi| = 37°$, and their erosive turbulence generation smoothing

648 out topography sizes. The spectral slump-down around k_T is statistically significant. However,

649 it also significantly varies between different sites, shifting about half an order of magnitude to

650 higher wavenumbers at Mount Josephine. This may relate with the dominance of 1.8-times

651 larger excursion length (~inverse wavenumber) of near-inertial waves in the East

652 Mediterranean, for fixed flow speed. Possibly, the excursion length of nonlinear breaking

653 internal waves is different for each site and different with dominant wave frequencies, being

654 inertial or tidal. Excursion length varies perhaps most with local flow speed in other areas.

655 For general GEBCO_2023 data from across the Mid-Atlantic Ridge in comparison with our

656 data, one finds also strict k^{-3} spectral fall-off rate and the spectral slump-down shifts by half

657 an order of magnitude to lower wavenumbers (not shown).

658

659 *3.3 Slope statistics*

660

661   The mean slope of seafloor topography calculated by Bell(1975a,b) at >100-m scales is

662 $3\pm1°$. In our two small areas around the same latitude (Fig. 2), the slope distribution varies

663 with length-scale; at slopes > 3°, the shorter the length-scales the steeper slopes are calculated

664 (Fig. 65). The 3°-slope is the median seafloor-slope value for our small East-Mediterranean

665 site, irrespective of scales used (Fig. 65a). The median seafloor-slope value for our small NE-

Formatted: Subscript

666   Atlantic site varies per scale and is about 4° at 1′-resolution and 5° at 0.25′-resolution (Fig.

667   6~~5~~b). These slopes are found for common mean N at z < -2000 m.

668   For most of the global ocean using a 1′-resolution, Costello et al. (2010) find that 9.4% of

669   the seafloors have a slope between 2 and 4°, 8.2% have a slope > 4° and 4.5% have a slope >

670   6°. From which we conclude that 3.7% have a slope between 4° and 6°. Recall that 75% of

671   the ocean area and 90% of its volume has seafloors between 3000 and 6000 m, where thus

672   most of these slope(percentage)s are.

673

674
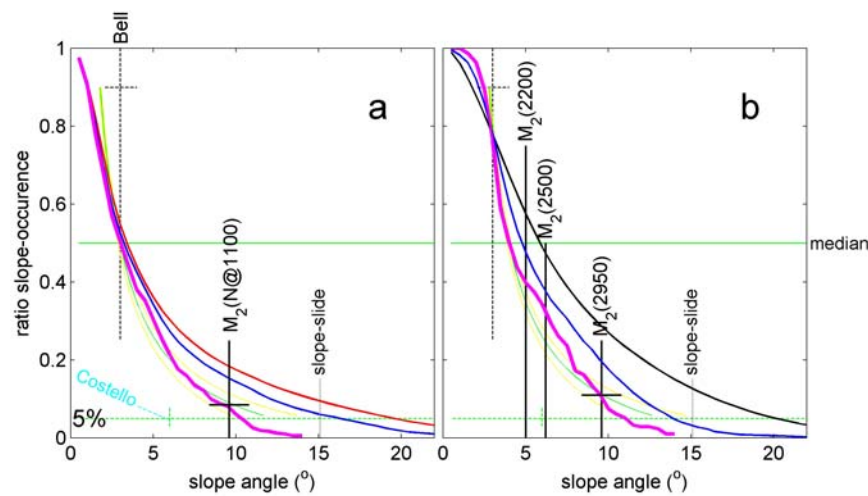
675   **Fig. 6~~5~~**. Seafloor ~~slope~~ statistics curves of ratio of slope~~angle excess~~ occurrence, percentage

676   of slopes being larger than particular slope angle (Section 2.2), for different seafloor-

677   elevation sampling scales. For comparison, ~~normalized~~ graph~~curve~~s are plotted for M_2

678   internal tid~~wav~~e characteristic slopes as a function of N against normalized N/N_{max}, one in

679   green using (1) and two in yellow using (2). The horizontal center green line indicates the

680   median, the lower horizontal dashed-green line indicates the 0.05(5%) level that is

681   required for (just-)supercritical slopes to generate sufficient global turbulence. Vertical

682   black-dashed lines indicate Bell (1975b)'s average slope of NE-Pacific abyssal hills and

683   the maximum slope before collapse of sediment packing 'slope-slide'. (a) From East-

684   Mediterranean map of Fig. 2a using three different scales for elevation slope-

685   computations: L = 1′ (magenta), 15″ (blue) and 3.75″ (red). Costello et al.'s (2010) range

686   of percentages is indicated in light-blue (see text). The semidiurnal lunar (M_2) internal tide

687   slope is indicated for local N at H = 1100 m, with corresponding error/spread in

688   characteristics value. (b) From NE-Atlantic map of Fig. 2b using L = 1′ (magenta), 14.5″

689   (blue) and 1.6″ (black). M_2-slopes for three different mooring sites are indicated as a

690   function of their H (m).

691

692   At our two sites, slopes are slightly steeper at 1′-resolution, and 5% of the seafloors have

693 slopes > 10°. For the East-Mediterranean, at 1′-resolution the (semidiurnal tidal) critical slope

694 is 9.6° for local N = 6.6×10^{-4} s^{-1}. This value of N is to within error the same value found for

695 N_v after volume-weighted averaging from (9) below z < -500 m of near-surface seasonal

696 stratification variation for open NE-Atlantic and Mariana Trench (Pacific Ocean) CTD

697 observations (Fig. 7b). It is noted that this volume-weighted averaging includes effects of

698 Antarctic Bottom Water, observed in the Mariana Trench profile. The value of N_v is three

699 times smaller than the mean buoyancy frequency used by Cacchione et al. (2002).

700

701
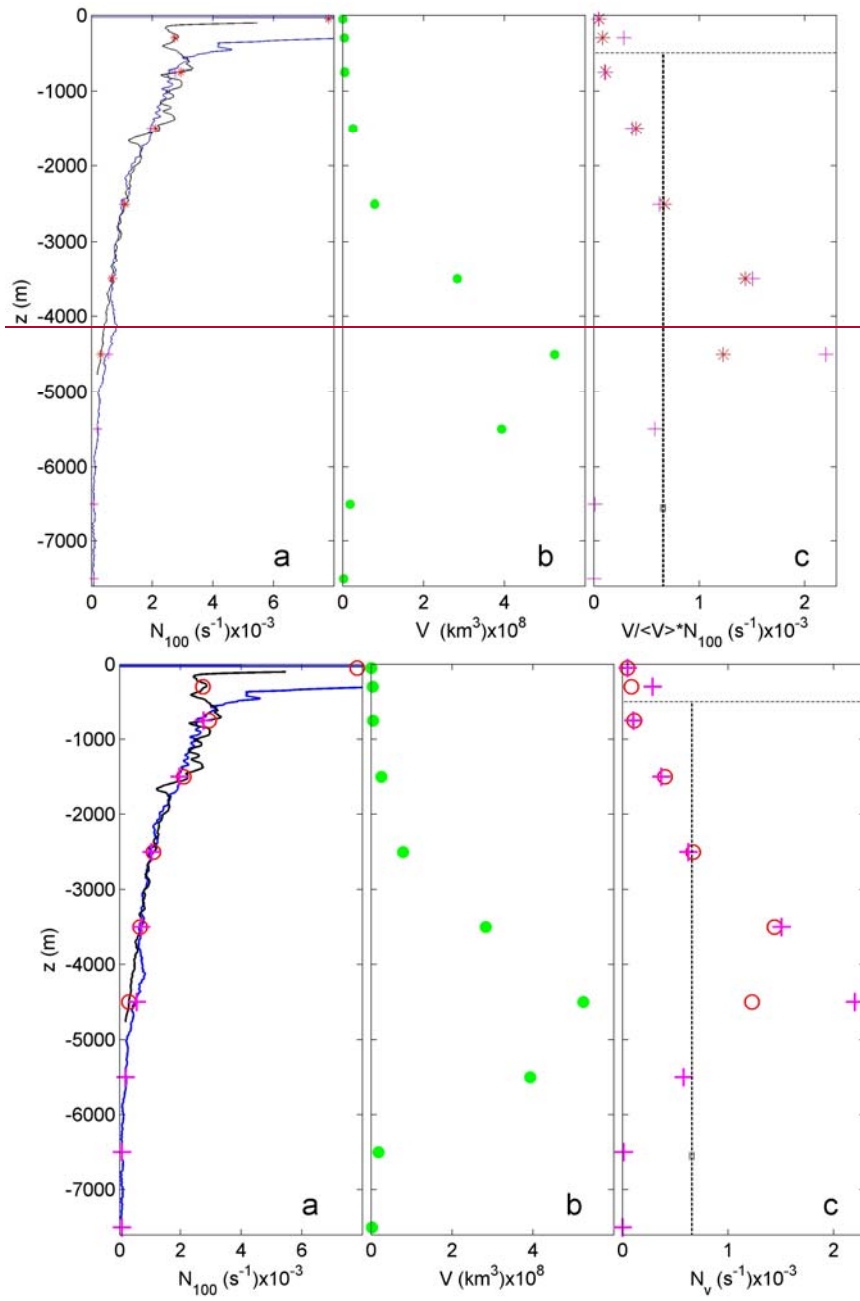
Fig. 7. Weighted function of buoyancy frequency as a function of the vertical. (a) Large-
100-m scale buoyancy frequency from NE-Atlantic, off Mount Josephine (green profile
with red circles) from the area in (van Haren et al. (2015), and over and inside

Mariana Trench (blue with magenta plusses) from (van Haren et al., 2017; van Haren et al., 2021). (b) Ocean volume $V(z)$ per depth zone, adapted from Costello et al. (2010) with depth zones defined in Costello et al. (2015). (c) Volume-weighted values of buoyancy frequency in (a) following (9) using $V(z)$ in (b). Note the relatively large value from around -4500 m in Mariana Trench data that is associated with Antarctic Bottom Water. Below z < -500 m, the vertical dashed line indicates mean value $\langle N \rangle = 6.6 \pm 0.2 \times 10^{-4}$ s^{-1}, for both profiles, with small error bar.

At this volume-weighted average N, associated supercritical slopes for semidiurnal lunar internal tide are found to occur for 5% of all slope values, i.e. 5% of all slopes are > 9.6° (Fig. 6a). This percentage is reached at an angle of 20° for 1.6″-resolution multibeam data of Mount Josephine (Fig. 6b). As this angle-value is steeper than that for sedimentary stability, its seafloor texture may thus foremost consist of hard substrate, which indeed has been observed in multibeam data for supercritical slopes (van Haren et al., 2015).

However, when computed at the larger 1′-resolution (magenta graphs in Fig. 6) one finds a 5%-transition for 11°, which is to within error the same slope for NE-Atlantic and East-Mediterranean multibeam data. Thus, seafloor slope statistics are identical to within error between our two sites at 1′-resolution. Recall that the 1′-resolution is close to the spectral transition length-scale $1/k_T$ (Figs. 4, 5), and close to the internal tidal (largest internal wave) excursion length for typical deep-sea flow speed. The characteristics (2) slope-range between 9 and 11° comprises the 10° seafloor-slope above which semidiurnal internal tides become supercritical at sites of the 3900-m mean ocean water depth given local N. Although this N is found around 1100 m in the East-Mediterranean, the approximate 2.5 times weaker N, compared with NE-Atlantic data at the same depth, associate with the lack of tides so that inertial energy is about 40% of total (inertial and tidal) internal wave energy found in the NE-Atlantic.

Although volume-weighted mean N and thus mean internal tidal characteristics slopes are found in the depth zone of mean ocean depth comprising 75% of the ocean area (Costello et al., 2010), the occurrence of 5% supercritical slopes diminishes local relatively weak

734 turbulence dissipation rates $O(10^{-9})$ m^2-s^{-3} to a small contribution <10% to maintain global

735 ocean stratification. However, the coincidence of 5% seafloor slopes with supercritical slopes

736 for volume-weighted mean N and N at mean ocean depth may reflect an ocean-wide balance

737 of internal wave-turbulence and topography interaction. Locally in the deep-sea, such

738 turbulence may have considerable influence for redistribution of sediment and nutrients.

739 Examples are short-term contributions of inertial waves generated by, e.g., large storms such

740 as typhoons. For standard mean 10^{-8} $m^2 s^{-3}$ over h = 200 m in H = 3900 m, 5% semidiurnal

741 tidal supercritical slopes yield a global contribution of 2.5×10^{-11} m^2-s^{-3}. A passing typhoon

742 may dissipate 10^{-7} $m^2 s^{-3}$ as observed (van Haren et al., 2020) over h = 200 m in H = 3100 m at

743 any slope, as basically all slopes are super-critical for a near-inertial wave characteristic.

744   Considering the more numerous moored T-sensor observations from the depth zone 100-

745 2000 m, which comprises 10% of the ocean area (Costello et al., 2010; 2015), the larger local

746 N yields 50% of local slopes to be supercritical (for semidiurnal tides), cf. Fig. 65. The

747 overall 50% of 10% = 5% supercritical slopes are sufficient to maintain the entire ocean

748 stratification over typical h = 100 m in average H =1000 m and observed turbulence

749 dissipation rate ε_{ho}. This is also the depth zone in which cold water corals (CWC) thrive

750 (United Nations, 2017). The suspension feeding CWC rely on nutrient supply via sufficiently

751 turbulent hydrodynamic processes.

752

753 **4 Discussion**

754   Cacchione et al. (2002) made calculations with water-level height mean N above a mean-

755 depth ocean seafloor, holding mean-N value constant for all z < -150 m. This is not

756 representing a realistic internal wave turbulence environment, because (1) N monotonically

757 decreases with depth (except under local conditions such as when Antarctic Bottom waters

758 are found near 4000 m), (2) internal waves refract so that local N has to be accounted for, (3)

759 internal waves predominantly break at sloping seafloor and not in the ocean-interior.

760   It is well established that internal tidal dissipation mainly occurs over steep topography

761 (e.g., Jayne et al., 2004). However, these authors emphasize that [global modelling efforts]

762 still lack a high resolution bathymetry data set to improve our ability to better quantify ocean

763 mixing, and understand its impact on the Earth's climate. It may well take considerable effort

764 and time until we have mapped the seafloor to the same detail as the surface of Mars (Smith,

765 2004).

766   Deep-ocean internal waves can be modelled to first order as linear waves and are found

767 ubiquitous throughout all seas and oceans. However, given their natural environment which is

768 not constant in space and time and their potential interactions with other water-flows they

769 divert considerably from linear, constant-frequency waves. First, the stratification-support

770 varies under internal wave straining, boundary flows and (sub-)mesoscale eddies, so that N

771 shows a relative variation of typically ±20%. Although semidiurnal internal tides are

772 dominant energetically, their variation in frequency alone provides 6% variations in slope of

773 characteristics. In the deep-sea, roughly the deeper half of all oceans, $N < 8f$, at mid-latitudes,

774 and full internal wave equations show a spread in internal tide characteristics of >15%. All

775 these natural variations, not counting variations in seafloor slope determination as a function

776 of length-scale, provide a relative error-range in dominant internal wave characteristics of 25-

777 50%.

778   It thus seems impossible to find a particular persistent critical slope for a given single

779 internal wave frequency on a 1′-scale, and which also ignores the highly nonlinear character

780 of dominant turbulence-generating upslope propagating bores, which are composed of

781 motions at many internal wave frequencies. Therefore, it is not surprising that most internal

782 wave generated turbulence occurs at (just) super-critical slopes, which provides a broader

783 slope- and thus frequency-range.

784   As the above relative uncertainty range of internal wave characteristics matches that of

785 relative error of about 33% (factor of 2) in mean turbulence dissipation rates, it reflects the

786 uncertainty in determining present-day percentage of supercritical slopes required to maintain

787 ocean stratification, being 5±1.5% for seas where internal tides dominate. This uncertainty

788 also sets the bounds for robustness of the internal wave-topography interactions: It is the

789 margin within which variations are expected to find sufficient feed-back not to disrupt the

790 system from some equilibrium.

791   If so, spiking any variations to this system must go beyond an energy variation of about

792 30%, which is larger than (the determination of) tidal variation but probably less than inertial

793 motions variations, say wind (Wunsch and Ferrari, 2004). In terms of stratification, 30% of

794 variation is feasible near the sea-surface via seasonal but also day-night variations, but is well

795 exceeding any natural stratification variations in the deep-sea, say for $z < -500$ m.

796   Suppose we can go beyond 30% variation, what will happen then? It takes at least

797 decades-centuries-millennia for the seafloor elevation to adapt to an equilibrium of

798 sufficiently supercritical slopes. If N increases by >30% uniformly throughout the ocean,

799 more (higher frequency) internal waves will be supported and internal tide characteristics will

800 become flatter. As a result, more (unaltered) seafloor slopes will become supercritical, which

801 will raise the amount of ocean turbulence. Perhaps by >30%. Increased turbulence means

802 more heat transport, hence a reduction of N that diminishes the initial 30%-increase. It goes

803 without saying that the opposite occurs in the event of a decrease in N.

804   Although being a meagre proof of evidence, we recall that the (East-)Mediterranean deep-

805 sea has a factor of 2-3 times weaker N than the tidally dominated NE-Atlantic Ocean at any

806 given depth. This factor is commensurate with the 2-3 times weaker near-inertial internal

807 wave energy compared with that of combined energy of internal tide and near-inertial waves.

808 Both sea-areas are in present-day equilibrium. As a result, it seems that it is not the buoyancy

809 (density stratification) variations that strongly disturb the equilibrium, but the external sources

810 of internal wave (kinetic energy).

811   (Just-)super-critical slopes are probably bounded by a maximum of 15° for sedimentary

812 slope-instability. At any rate, the super-critical seafloor slopes allow development of upslope

813 propagating bores and rapid restratification of the back-and-forth sloshing internal tides. In

814 contrast with foreward wave-breaking at a beach, internal tides break backwards at a slope

815 (van Haren and Gostiaux, 2012). This may explain a lack of clear swash, i.e., while upslope

816 propagating bores may be considered as uprush, a clear vigorous backwash is not observed

817 during the downslope warming tidal phase near the seafloor in moored T-sensor data. This
818 demonstrates a discrepancy with the 2-D modelling of Winters (2015). While in the model
819 most intense turbulence is found near the seafloor during the downslope phase expelling into
820 the interior, ocean observations demonstrate largest turbulence around the upslope
821 propagating backwards breaking bore, with the bore sweeping material up from the seafloor
822 (Hosegood et al., 2004). Probably some 3D- or rotational aspect is important for ocean
823 internal wave breaking, yet to be modelled.

824   We have considered a combination of seafloor elevation and internal wave turbulence data
825 to revisit the interaction between topography and water flows in the deep-sea. From various
826 perspectives including turbulence values, vertical density stratification, (water) depth zones,
827 and seafloor and internal wave slopes and scale-lengths it is found that interaction is relatively
828 stable, whereby mainly internal tides and near-inertial waves shape the topography to within
829 30% variability.

830

831 **5 Conclusions**

832   The median value of seafloor slope of 3±0.2° from multibeam echosounder and satellite
833 data from NE-Atlantic, mid-Atlantic Ridge and East-Mediterranean sites closely matches the
834 half-a-century-ago established rms-mean slope of 3±1° from single-beam echosounder data
835 across NPE-Pacific abyssal hills (Bell, 1975a,b). Our result is found only weakly dependent
836 of scale, which we varied between 0.027′ and 1′. It lends some robustness to the
837 determination of seafloor slopes, for horizontal scales that match dominant internal wave
838 excursion lengths.

839   The average spectral fall-off rate of seafloor elevation is found steeper than Bell's
840 (1975a,b), which indicates a non-uniform distribution of scales instead of a uniform
841 distribution as previously suggested. In particular, the spectral slump-down around a length-
842 scale of 2 km is noted, which suggests a lack of seafloor elevation shaped by the largest
843 internal wave excursion length dissipating its energy into turbulence creating sediment

844   erosion. This spectral slump-down is found in seafloor elevation data from both the NE-

845   Atlantic, where semidiurnal internal tides prevail, and, at somewhat smaller values, from the

846   East-Mediterranean, where tides are small and near-inertial motions that have 1.8 times larger

847   length scales dominate internal waves. In the East-Mediterranean, the buoyancy frequency is

848   found smaller than at corresponding depths in the NE-Atlantic, which is commensurate with

849   the contribution of internal tides (and lack thereof).

850   Recent moored high-resolution T-sensor data demonstrated that internal wave breaking is

851   found most vigorously above seafloor slopes that are supercritical rather than much more

852   limiting critical for (semidiurnal) internal tides, with local turbulence dissipation rate $> 10^{-7}$

853   m^2s^{-3} in depth zone $100 < H < 2200$ m (NE-Atlantic). This depth zone hosts most of cold-

854   water corals that depend on vigorous turbulence for nutrient supply. Our seafloor statistics

855   show that 50% of the slopes are supercritical for stratification in this depth zone, which

856   compensates for the depth zone's occupation of only 10% of ocean area. As a result, we find

857   that internal wave breaking at $5\pm1.5\%$ of slopes suffices to maintain global ocean density

858   stratification.

859   In greater depth zones, internal wave breaking is generally less turbulent contributing

860   <10% to maintain global stratification mainly due to steeper internal tidal characteristics

861   slopes. Even in the deep-sea however, 5% of seafloor slopes coincide with supercritical slopes

862   for volume-weighted mean N_v, and N at mean ocean depth, supporting an ocean-wide balance

863   of topography and internal wave-turbulence interaction. Turbulence may be locally important

864   for the redistribution of heat, nutrients, and oxygen, e.g., during the passage of typhoons

865   generating near-inertial waves as most seafloor slopes are supercritical for (one characteristic

866   of) such waves, also in great depth zones.

867

868   *Data availability.* Seafloor elevation data are extracted from depositories

869   https://www.gebco.net and https://emodnet.ec.europa.eu/en/bathymetry. Raw East-

Formatted: Subscript

870 Mediterranean CTD data supporting the results of this study are available in database

871 https://data.mendeley.com/datasets/6td5dxf6bj/1.

872

873 *Author contribution:* HvH designed the experiments, while HvH and HdH carried them out.

874 HvH focused on the oceanographic part, HdH on the topographic and sedimentology part.

875 HdH verified that figures are colour-blind friendly HvH prepared the manuscript with

876 contributions from HdH.

877

878 *Competing interests.* The authors have no conflicts to disclose.

879

880 *Ackowledgments.* NIOZ T-sensors were supported in part by NWO, the Netherlands

881 Organization for the advancement of science. We thank NIOZ-MRF and the captains and

882 crews of the R/V's Pelagia and Meteor, as well as from numerous other research vessels we

883 joined, for their very helpful assistance during mooring construction and deployment.

884

885   **References**

886   Alford, M. H.: Improved global maps and 54-year history of wind-work on ocean inertial

887   motions, Geophys. Res. Lett., 30, 1424, 2003.

888   Armi, L.: Effects of variations in eddy diffusivity on property distributions in the oceans, J.

889   Mar. Res., 37, 515-530, 1979.

890   Bell, T. H. Jr.: Topographically generated internal waves in the open ocean, J. Geophys. Res.,

891   80, 320-327, 1975a.

892   Bell, T. H. Jr.: Statistical features of sea-floor topography, Deep-Sea Res., 22, 883-892,

893   1975b.

894   Cacchione D. A., and Southard, J. B.: Incipient sediment movement by shoaling internal

895   gravity waves, J. Geophys. Res., 79, 2237-2242, 1974.

896   Cacchione, D. A., and Wunsch, C.: Experimental study of internal waves over a slope, J.

897   Fluid Mech., 66, 223-239, 1974.

898   Cacchione, D. A., Pratson, L. F., and Ogston, A. S.: The shaping of continental slopes by

899   internal tides, Science, 296, 724-727, 2002.

900   Chen, H., Zhang, W., Xie, X., Gao, T., Liu, S., Ren, J., Wang, D., and Su, M.: Linking

901   oceanographic processes to contourite features: Numerical modelling of currents

902   influencing a contourite depositional system on the northern South China Sea margin,

903   Mar. Geol., 444, 106714, 2022.

904   Costello, M. J., Cheung, A., and de Hauwere, N.: Surface area and the seabed area, volume,

905   depth, slope, and topographic variation for the world's seas, oceans, and countries,

906   Environ. Sci. Technol., 44, 8821-8828, 2010.

907   Costello, M. J., Smith, M., and Fraczek, W.: Correction to Surface area and the seabed area,

908   volume, depth, slope, and topographic variation for the world's seas, oceans, and

909   countries, Environ. Sci. Technol., 49, 7071-7072, 2015.

910   Dillon, T. M.: Vertical overturns: a comparison of Thorpe and Ozmidov length scales, J.

911   Geophys. Res., 87, 9601-9613, 1982.

912   Dushaw, B. D.: Mapping low-mode internal tides near Hawaii using TOPEX/POSEIDON
913   altimeter data, Geophys. Res. Lett., 29, 1250, 2002.

914   Eriksen, C. C.: Observations of internal wave reflection off sloping bottoms, J. Geophys.
915   Res., 87, 525-538, 1982.

916   Eriksen, C. C.: Implications of ocean bottom reflection for internal wave spectra and mixing.
917   J. Phys. Oceanogr., 15, 1145-1156, 1985.

918   Ferrari, R., Mashayek, A., McDougall, T. J., Nikurashin, M., and Campin, J.-M.: Turning
919   ocean mixing upside down, J. Phys. Oceanogr., 46, 2229-2261, 2016.

920   Garrett, C.: The role of secondary circulation in boundary mixing, J. Geophys. Res., 95, 3181-
921   3188, doi:10.1029/JC095iC03p03181, 1990.

922   Gerkema, T., Zimmerman, J. T. F., Maas, L. R. M., and van Haren, H.: Geophysical and
923   astrophysical fluid dynamics beyond the traditional approximation, Rev. Geophys., 46,
924   RG2004, doi:10.1029/2006RG000220, 2008.

925   Gregg, M. C.: Scaling turbulent dissipation in the thermocline, J. Geophys. Res., 94, 9686-
926   9698, 1989.

927   Hosegood, P., Bonnin, J., and van Haren, H.: Solibore-induced sediment resuspension in the
928   Faeroe-Shetland Channel, Geophys. Res. Lett., 31, L09301, doi:10.1029/2004GL019544,
929   2004.

930   Jayne, S. R., St. Laurent, L. C., and Gille, S. T.: Connections between ocean bottom
931   topography and Earth's climate, Oceanography, 17(1), 65-74, 2004.

932   King, B., Stone, M., Zhang, H. P., Gerkema, T., Marder, M., Scott, R. B., and Swinney, H. L.:
933   Buoyancy frequency profiles and internal semidiurnal tide turning depths in the oceans, J.
934   Geophys. Res., 11, C04008, doi:10.1029/2011JC007681, 2012.

935   Klymak J. M., and Moum, J. N.: Internal solitary waves of elevation advancing on a shoaling
936   shelf, Geophys. Res. Lett., 30, 2045, doi:10.1029/2003GL017706, 2003.

937   Kunze, E.: Near-inertial wave propagation in geostrophic shear, J. Phys. Oceanogr., 15, 544-
938   565, 1985.

939   Kunze, E.: Internal-wave-driven-mixing: Global geography and budgets, J. Phys. Oceanogr.,
940   47, 1325-1345, 2017.

941   LeBlond, P., and Mysak, L. A.: Waves in the Ocean, Elsevier, Amsterdam, 602 pp, 1978.

942   Legg, S., and Adcroft, A.: Internal wave breaking at concave and convex continental slopes,
943   J. Phys. Oceanogr., 33, 2224-2246, 2003.

944   Munk, W. H.: Abyssal recipes, Deep-Sea Res., 13, 707-730, 1966.

945   Munk W., and Wunsch, C.: Abyssal recipes II: Energetics of tidal and wind mixing, Deep-Sea
946   Res. I, 45, 1977-2010, 1998.

947   Oakey, N. S.: Determination of the rate of dissipation of turbulent energy from simultaneous
948   temperature and velocity shear microstructure measurements, J. Phys. Oceanogr., 12,
949   256-271, 1982.

950   Osborn, T. R.: Estimates of the local rate of vertical diffusion from dissipation measurements,
951   J. Phys. Oceanogr., 10, 83-89, 1980.

952   Polzin, K. L., Toole, J. M., Ledwell, J. R., and Schmitt, R. W.: Spatial variability of turbulent
953   mixing in the abyssal ocean, Science, 276, 93-96, 1997.

954   Puig, P., Ogston, A. S., Guillén, J., Fain, A. M. V., and Palanques, A.: Sediment transport
955   processes from the topset to the foreset of a crenulated clinoform (Adriatic Sea), Cont.
956   Shelf Res., 27, 452-474, 2007.

957   Ray, R. D., and Zaron, E. D.: M_2 internal tides and their observed wavenumber spectra from
958   satellite altimetry, J. Phys. Oceanogr., 46, 3-22, 2016.

959   Rebesco, M., Hernández-Molina, F. J., van Rooij, D., and Wåhlin, A.: Contourites and
960   associated sediments controlled by deep-water circulation processes: State-of-the-art and
961   future considerations, Mar. Geol., 352, 111-154, 2014.

962   Sarkar, S., and Scotti, A.: From topographic internal gravity waves to turbulence, Ann. Rev.
963   Fluid Mech., 49, 195-220, 2017.

964   Schuster, H. G.: Deterministic Chaos: An Introduction, Physik Velag, Weinheim, Germany,
965   220 pp, 1984.

966   Smith, W. H. F.: Introduction to this special issue on bathymetry from space, Oceanography,

967   17(1), 6-7, 2004.

968   Smith, W. H. F., and Sandwell, D. T.: Global seafloor topography from satellite altimetry and

969   ship depth soundings, Science, 277, 1957-1962, 1997.

970   St. Laurent, L., Alford, M. H., and Paluszkiewicz, T.: An introduction to the special issue on

971   internal waves, Oceanography 25(2), 15-19, 2012.

972   Thorpe S. A.: Turbulence and mixing in a Scottish Loch, Phil. Trans. Roy. Soc. A, 286, 125-

973   181, 1977.

974   Thorpe, S. A.: Transitional phenomena and the development of turbulence in stratified fluids:

975   a review, J. Geophys. Res., 92, 5231-5248, 1987.

976   Trincardi, F., and Normark, W. R.: Sediment waves on the Tiber pro-delta slope, Geo-Mar.

977   Lett., 8, 149-157, 1988.

978   United Nations, ed.: Cold-Water Corals, In: The First Global Integrated Marine Assessment:

979   World Ocean Assessment I. Cambridge University Press, 803-816, 2017.

980   van Haren, H.: Philosophy and application of high-resolution temperature sensors for

981   stratified waters, Sensors, 18, 3184. doi:10.3390/s18103184, 2018.

982   van Haren, H.: Open-ocean interior moored sensor turbulence estimates, below a Meddy,

983   Deep-Sea Res. I, 144, 75-84, 2019.

984   van Haren, H., and Gostiaux, L.: Energy release through internal wave breaking,

985   Oceanography 25(2), 124-131, 2012.

986   van Haren, H., and Puig, P.: Internal wave turbulence in the Llobregat prodelta (NW

987   Mediterranean) under stratified conditions: A mechanism for sediment waves generation?

988   Mar. Geol., 388, 1-11, 2017.

989   van Haren, H., Maas, L., Zimmerman, J. T. F., Ridderinkhof, H., and Malschaert, H.: Strong

990   inertial currents and marginal internal wave stability in the central North Sea, Geophys.

991   Res. Lett., 26, 2993-2996, 1999.

992   van Haren, H., Cimatoribus, A. A., and Gostiaux, L.: Where large deep-ocean waves break,

993   Geophys. Res. Lett., 42, 2351-2357, doi:10.1002/2015GL063329, 2015.

994   van Haren, H., Cimatoribus, A. A., Cyr, F., and Gostiaux, L.: Insights from a 3-D temperature

995   sensors mooring on stratified ocean turbulence, Geophys. Res. Lett., 43, 4483-4489,

996   doi:10.1002/2016GL068032, 2016.

997   van Haren, H., Berndt, C., Klaucke, I.: Ocean mixing in deep-sea trenches: new insights from

998   the Challenger Deep, Mariana Trench, Deep-Sea Res. I, 129, 1-9, 2017.

999   van Haren, H., Chi, W.-C., Yang, C.-F., Yang, Y. J., and Jan, S.: Deep sea floor observations

1000   of typhoon driven enhanced ocean turbulence, Progr. Oceanogr., 184, 102315, 2020.

1001   van Haren, H., Uchida, H., Yanagimoto, D.: Further correcting pressure effects on SBE911

1002   CTD-conductivity data from hadal depths, J. Oceanogr., 77, 137-144, 2021.

1003   van Haren, H., Mienis, F., and Duineveld, G.: Contrasting internal tide turbulence in a

1004   tributary of the Whittard Canyon, Cont. Shelf Res. 236, 104679, 2022.

1005   Voulgaris, G., and Collins, M. B.: Sediment resuspension on beaches: response to breaking

1006   waves, Mar. Geol., 167, 167-187, 2000.

1007   Watanabe, M., and Hibiya, T.: Global estimates of the wind-induced energy flux to inertial

1008   motions   in   the   surface   mixed   layer,   Geophys.   Res.   Lett.,   29,   1239,

1009   doi:10.1029/2001GL014422, 2002.

1010   Winters, K. B.: Tidally driven mixing and dissipation in the stratified boundary layer above

1011   steep submarine topography, Geophys. Res. Lett., 42, 7123-7130, 2015.

1012   Wüst, G.: The Stratosphere of the Atlantic Ocean. Scientific Results of the German Atlantic

1013   Expedition of the Research Vessel Meteor, 1925-27, Vol. VI, Section 1, English

1014   translation, W. J. Emery (ed.). Amerind Pub. Co., New Delhi, 1978, 1935.

1015   Wunsch, C.: On oceanic boundary mixing, Deep-Sea Res., 17, 293-301, 1970.

1016   Wunsch, C., and Ferrari, R.: Vertical mixing, energy, and the general circulation of the

1017   oceans, Annu. Rev. Fluid Mech., 36, 281-314, 2004.

1018   Wunsch, C.: Modern observational physical oceanography: Understanding the global ocean,

1019   Princeton University Press. 512 pp, 2015.

1020